अतिचालक क्यूबिट

13

समायोजनीय युग्मक का अभिकल्पन : दो क्यूबिट के साथ किए गए अनुकरण

*सुमिता सुरा[1], दिपक पास्टे[1], प्रवीण कुमार सुग्गिसेट्टी[1], एम.वाई. दीक्षित[1], गोपाल जोशी[1], विजय राघवन[2]

[1]*त्वरक नियंत्रण प्रभाग, भाभा परमाणु अनुसंधान केंद्र (भापअ केंद्र), ट्रांबे-400085, भारत*
[2]*क्वांटम मापन और नियंत्रण (क्यूएमएसी) संघनित पदार्थ भौतिकी और सामग्री विज्ञान विभाग टाटा मूलभूत अनुसंधान संस्थान (टीआईएफआर), मुंबई*

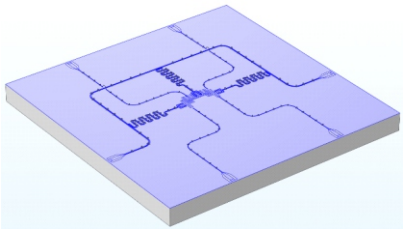

दो-क्यूबिट समायोजनीय युग्मक हेतु चिप संरचना

सारांश

एक समायोजनीय युग्मक (ट्यूनबल क्पलर) के मध्यस्थता के अधीन दो-क्यूबिट वाले क्वांटम प्रोसेसर के विभिन्न घटकों को डिजाइन करने के लिए विद्युत चुंबकीय और क्वांटम अनुकरण किया गया है। इन अनुकरणों के माध्यम से, प्रणाली के वांछित हैमिल्टनियन को प्राप्त करने के लिए विभिन्न डिजाइन पैरामीटरों की गणना की गई है। क्यूबिट्स के बीच स्थिर अवांछित ZZ युग्मन के दमन के लिए समायोजनीय युग्मक की आवृत्ति सीमा की पहचान की गई है, और समायोजनीय युग्मक का उपयोग करके क्यूबिट्स के बीच स्थितियों की अदला-बदली का प्रदर्शन किया गया है।

Superconducting Qubits

13

Designing a Tunable Coupler: Simulations with Two Qubits

Sumita Sura[1], Deepak Paste[1], Praveen Kumar Suggisetti[1], M. Y. Dixit[1], Gopal Joshi[1] and R. Vijayaraghavan[2]

[1]*Accelerator Control Division, Bhabha Atomic Research Centre (BARC), Trombay-400085, INDIA*
[2]*Quantum Measurement and Control (QuMaC) Laboratory, Department of Condensed Matter Physics and Materials Science, Tata Institute of Fundamental Research (TIFR), Mumbai*

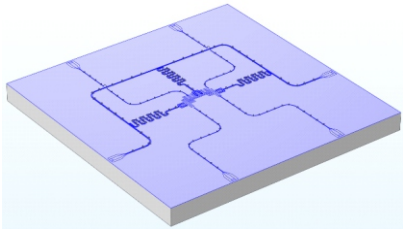

Chip architecture for two-qubit tunable coupler

ABSTRACT

Electromagnetic and Quantum simulations have been performed to design different components of a quantum processor having two qubits mediated via a tunable coupler. Through these simulations, various design parameters have been extracted to achieve the desired Hamiltonian of the system. Frequency range of tunable coupler has been identified to suppress the static parasitic ZZ coupling between qubits, and swapping of states between the qubits, using the tunable coupler, has been demonstrated.

KEYWORDS: *Superconducting qubits, Tunable coupler architecture, Microwave simulation*

**Author for Correspondence: Sumita Sura*
E-mail: sumitasura@barc.gov.in

Introduction

Superconducting quantum circuits have demonstrated promising potential in various applications [1-5]. These circuits are solid state devices with macroscopic dimensions. The Josephson junction element [6] introduces non-linear inductance, thus making quantum energy levels to be unequally spaced. By employing lowest two energy levels as quantum bit (qubit), superconducting qubits have shown immense potential for information processing [7]. Manipulation and readout of qubit states is achieved through the concepts derived from circuit quantum electrodynamics (cQED) [8], where microwave pulses are employed to control and read qubit states. Advancement in the field of microwaves and microfabrication has enabled integration of these qubits into chips [9].

Despite advancements, performance of these devices is limited due to unwanted parasitic couplings and noise [10]. To overcome the challenge posed by parasitic coupling, an additional circuit element is inserted between two qubits to control the interactions. This element, known as tunable coupler, removes the parasitic coupling by destructively interfering direct interaction between qubits with the virtual interaction mediated by the states of the coupler [11]. Furthermore, by tuning the frequency of the tunable coupler, desired coupling strength between qubits can be generated, enabling implementation of fast gates [11-12].

This article presents results of the electromagnetic simulations performed on a two-qubit tunable coupler system including readout and control channels. Through numerical simulations, effect of change in the coupler frequency on the coupling between qubits is obtained. Also, the always on static ZZ parasitic [12-13] interaction has been estimated. Two qubit iSwap gate operation using tunable coupler has been demonstrated.

System architecture

Layout of the quantum chip is shown in Fig.1. It consists of two xmons coupled via a transmon acting as Coupler [12]. Ease of connections and minimization of cross talk have been important considerations in deciding the orientation of remaining parts of the chip. Specifically, the quantum chip consists of following components:

- Two xmon qubits Q_1 and Q_2 on silicon substrate, Q_1 is fixed frequency and Q_2 incorporates flux tunablity,

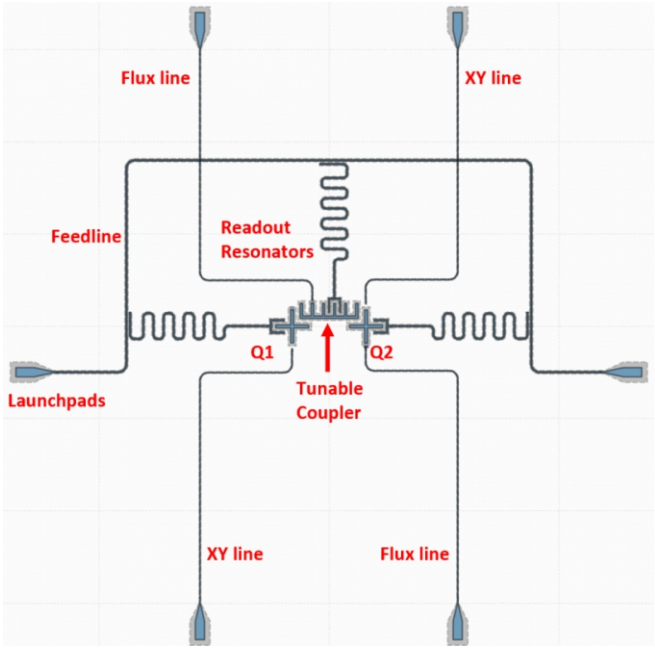

Fig.1: Layout of Quantum Chip.

- Two XY control lines, capacitively coupled to Q_1 and Q_2, and a flux line inductively coupled to Q_2,
- A flux tunable transmon as Coupler, and
- Three readout resonators capacitively coupled to Q_1, Q_2 and Coupler, respectively, and inductively coupled to a 50 Ω transmission line.

The frequency of the xmon qubits, $Q_1$and Q_2, is kept close to 4 GHz. Geometrical parameters of all the three qubits have been finalized based on simulations. Open-source package, Qiskit Metal [14], has been used extensively for design and simulation.

Electromagnetic Simulations

Qubit parameters

An E_j over E_c ratio more than 50, anharmonicity close to 200 MHz and frequencies of Q_1 and Q_2 xmons about 4 GHz, have guided the design pertaining to Q_1 and Q_2. Capacitance analysis has been performed to get the required shunt capacitances. By optimizing the geometries, Q_1 and Q_2 qubit

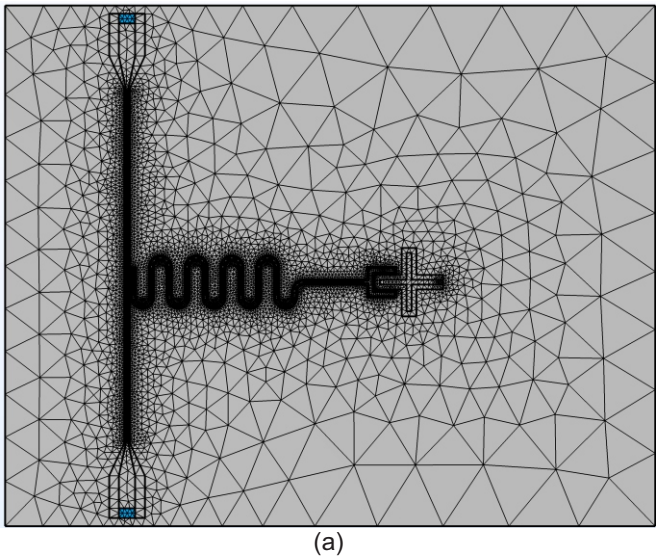

(a)

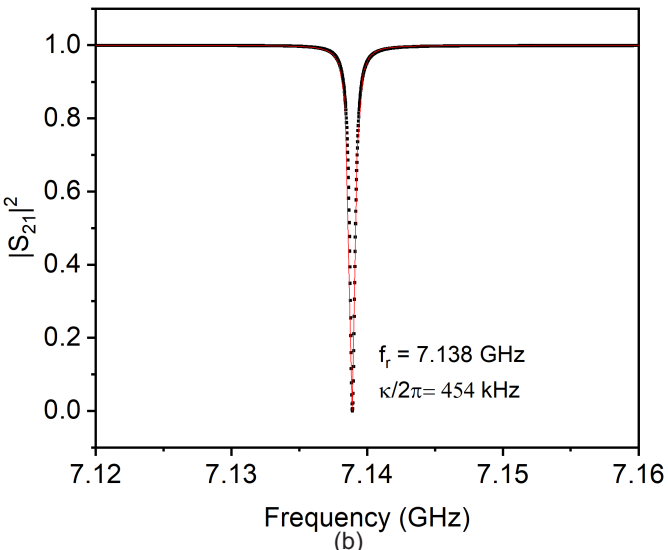

(b)

Fig.2: (a) Mesh distribution for a resonator-qubit structure (b) $|S_{21}|^2$ vs frequency.

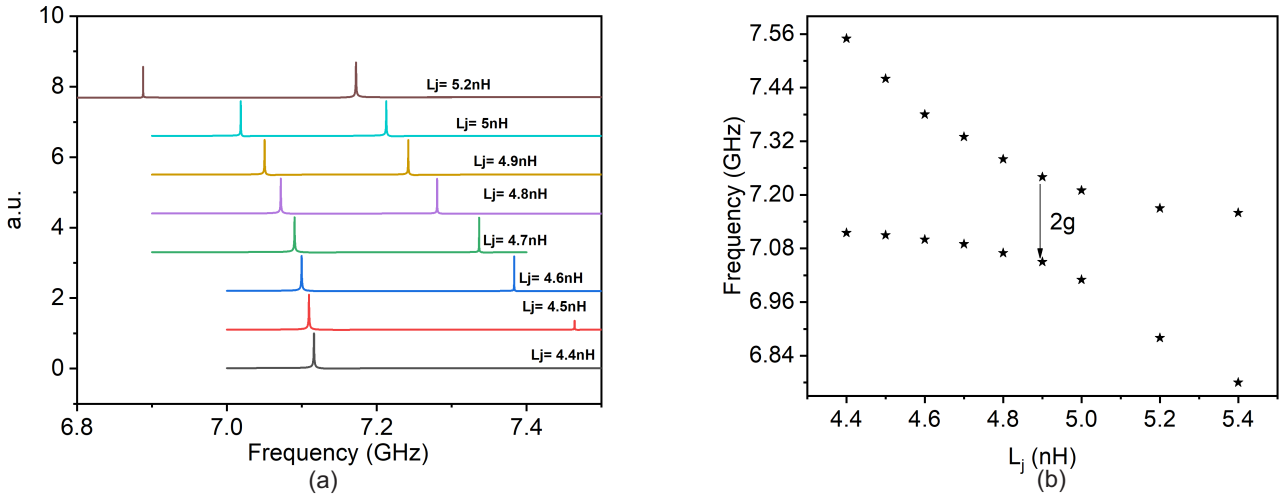

Fig.3: (a) $|S_{21}|^2$ as a function of the frequency for different inductance value L_j, which determines the qubit frequency, (b) avoided crossing plot.

frequencies (f_1, f_2) equal to 4.1 and 4.2 GHz, and qubit anharmonicity (α) equal to 217 MHz, are obtained.

Readout resonator

A quarter-wavelength (λ/4) resonator has been designed for dispersive readout of qubit state. This resonator is capacitively coupled to qubit and inductively coupled to a transmission feedline. The resonator frequency, which determines its length, is aimed to be close to 7 GHz. The coupling of resonator to feedline is so selected that the line-width of resonator is close to 500kHz. Through simulations, transmission coefficient S_{21} of feedline coupled to the resonator-xmon system, shown in Fig.2 (a), has been studied. By fitting Lorentzian function to $|S_{21}|^2$, as shown in Fig.2 (b), the resonator frequency is obtained as 7.138 GHz. Full-width-half-maximum of the peak, k/2π Hz, which determines how fast the photons in the resonator decay, is estimated as 454 kHz.

The coupling strength, g/2π, of resonator to qubit has been estimated from the gap between qubit and resonator frequency at avoided crossing. The qubit frequency is changed by changing the inductance parameter of the qubit, L_j, as shown in Fig.3 (a). By fitting a second order polynomial to the avoided crossing, the coupling strength g/2π has been estimated to be about 99 MHz. The simulated avoided crossing plot has been shown in Fig.3 (b).

The readout scheme, where coupling strength g/2π is very less than frequency detuning between resonator and qubit, is known as dispersive readout. In this regime, the state of qubit induces a frequency shift in coupled resonator. This state dependent frequency shift, $\chi/2\pi$, known as dispersive strength of resonator, has been calculated to be about 156 kHz [15]. This coupling of resonator to qubit also induces Purcell decay in qubit states. This decay rate of the qubit, $\gamma/2\pi$, has

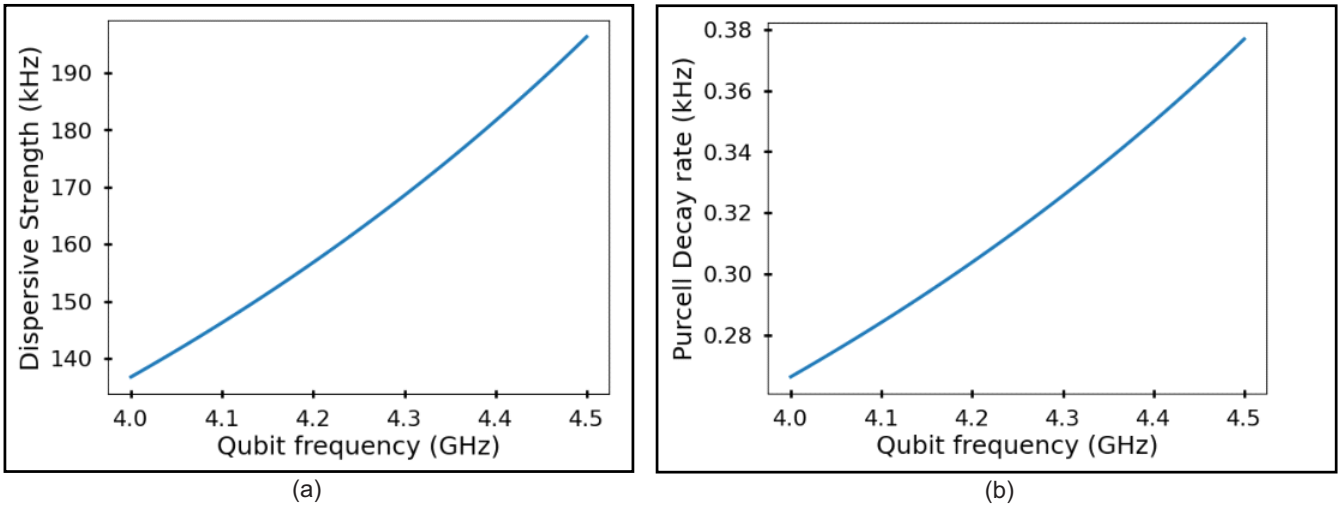

Fig.4: (a) Dispersive strength, (b) Purcell decay rate with qubit frequency.

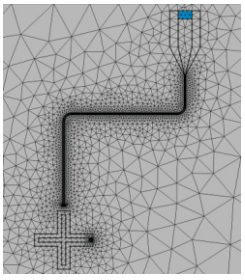

Fig.5: Mesh distribution for a XY Line-qubit structure at 40 um gap.

Table 1: Coupling capacitances and decay time T_1 at different gaps.

Gap between qubit and XY control line (um)	Coupling capacitance (aF)	Decay time T_1 (us)
15	72.8	169
30	43.8	374
40	33.6	546

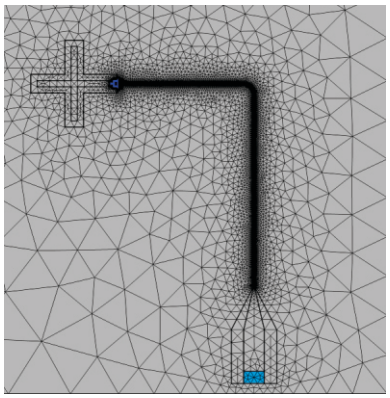

Fig.6: Mesh distribution for the Flux line inductively coupled to squid of qubit.

been calculated using formula given in reference [15] to be 0.30 kHz. This formula used for the decay rate is based on single mode approximation of the readout resonator. Detailed EM simulations are planned to get more accurate results at large detuning. The variations in $\chi/2\pi$ and $\gamma/2\pi$ have been plotted with respect to qubit frequency in Fig.4 (a) and (b), respectively. For qubit frequency range 4 to 4.5 GHz, the dispersive strength ranges from 135 to 195 kHz and the Purcell decay rate ranges from 0.26 kHz to 0.37 kHz, as shown in Fig.4.

Control lines

These are 50 Ω transmission lines which carry microwave pulses to manipulate state of qubit. For the present design, these include XY control lines to change states of qubit, and Flux control line to change frequency of the qubit. Choosing optimum coupling parameter to the qubit is a crucial step as too strong coupling will induce decoherence/noise channel and a too weak coupling will degrade the performance of qubit.

(a) XY control line: The XY control line is capacitively coupled to

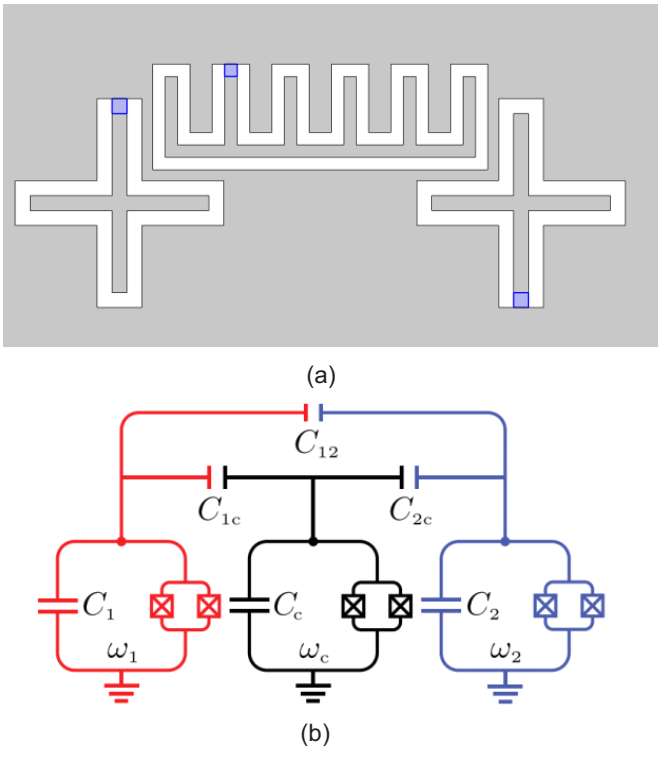

Fig.7: (a) Physical arrangement of Tunable coupler capacitively coupled to qubits, (b) Equivalent circuit diagram.

Table 2: Capacitance values obtained from Quasi-electrostatic simulations.

Symbol	Capacitance (fF)
C_1	96.60
C_2	96.60
C_c	191.29
C_{1c}	3.84
C_{2c}	3.85
C_{12}	0.1125

the qubit. The coupling capacitance is optimized parameter to minimize the decay while ensuring reasonable drive strength for gate implementation. The simulations have been carried out to get this optimal capacitance by varying gap between qubit and control line. By using black box quantization method [16] we have simulated the decay time at each gap position. Estimated capacitances and decay time of qubit due to energy loss through XY control line is listed in Table 1. We have obtained a decay time of 546 μs at 40um gap where the coupling capacitance is 33 aF. This gives an excitation π-pulse magnitude as –67.5 dBm [17].

(b) Flux control line: The flux line is inductively coupled to the SQUID of qubit. Sufficient mutual inductance between the flux line and the qubit SQUID loop needs to be ensured. The coupling of flux line is optimized to achieve a mutual inductance of 1.08 pH.

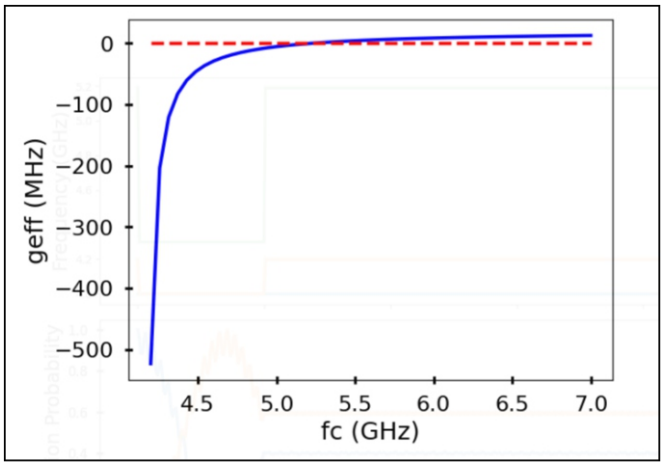

Fig.8: Effective coupling strength between qubits at different coupler frequency.

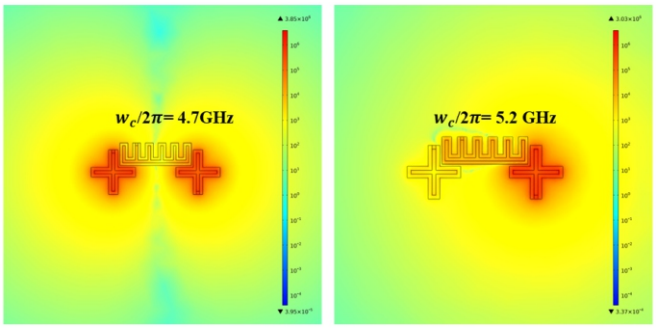

Fig.9: Electric field distribution at coupler frequency 4.7 GHz and 5.2 GHz for Q_2 resonant mode

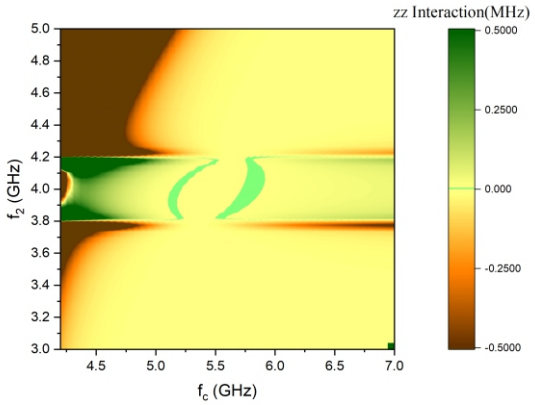

Fig.10: Parasitic ZZ interaction with Coupler and Q_2 frequency.

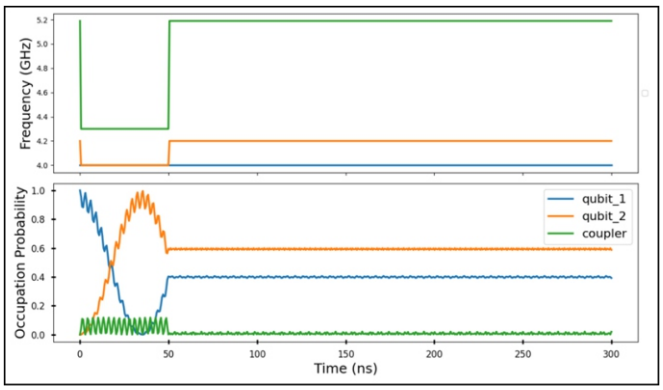

Fig.11: State evolution of Q_1, Q_2 and Coupler with time.

Tunable coupler

In the present case a transmon qubit has been taken as tunable coupler. The physical arrangement and the equivalent circuit of the qubits with the tunable coupler [12] is shown in Fig.7 (a) and 7 (b), respectively. In this scheme the two qubits are directly coupled with each other via capacitance networks, and indirectly via the states of tunable coupler. The coupler is capacitively coupled to the qubits with capacitance C_{1c} and C_{2c} giving rise to coupling strength of g_1 and g_2, respectively. The direct capacitance between the qubits is given by C_{12} and contributes to the direct coupling given by g_{12}. With coupler frequency higher than the frequencies of qubits, the coupling through the coupler states is negative. The coupler has been designed to have weak anharmonicity of about 90 MHz and frequency tunability from 4 to 5.5 GHz. The coupling capacitances between the qubit and the coupler have been selected to achieve zero coupling around 5.2 GHz of the coupler frequency. The values of the required capacitances are obtained from quasi-static simulations and are listed in Table 2.

The effective coupling strength between the qubits Q_1 and Q_2 is estimated using the formula given in reference [11] and plotted against coupler frequency in Fig.8. It is observed that at coupler frequency, $\omega_c/2\pi$, of about 5.19GHz, effective coupling between the qubits become zero. Fig.9 shows the electric field distribution with coupler frequency at 4.7 GHz and 5.2 GHz, respectively.

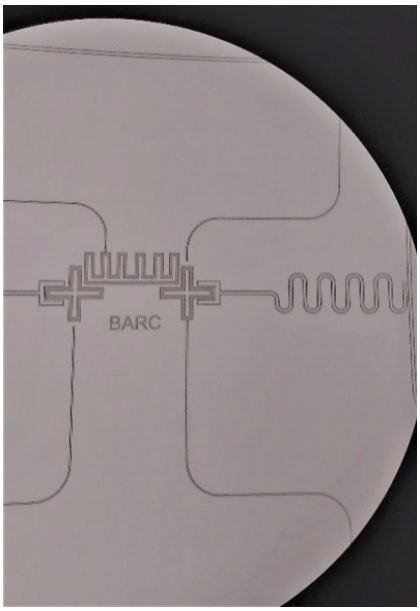

Fig.12: (a) Optical image of fabricated device.

Quantum simulations

By employing open-source python library Quantum Toolbox in Python (QuTiP) [18], evolution of quantum states with time has been simulated. The system Hamiltonian consists of sum of Hamiltonians of individual qubits and coupler, and interaction terms between them. Hamiltonian has been modelled as duffing oscillator [11]. For present simulations readout resonators and control lines have been removed. The Hamiltonian is given by,

$$H = \sum_{i=1,2,c} (\omega_i \hat{c}_i^\dagger \hat{c}_i + \alpha_i \hat{c}_i^\dagger \hat{c}_i^\dagger \hat{c}_i \hat{c}_i) + \sum_{i=1,2} g_i (\hat{c}_i^\dagger \hat{c}_c + \hat{c}_c^\dagger \hat{c}_i - \hat{c}_i^\dagger \hat{c}_c^\dagger - \hat{c}_i \hat{c}_c) + g_{12}(\hat{c}_1^\dagger \hat{c}_2 + \hat{c}_2^\dagger \hat{c}_1 - \hat{c}_i^\dagger \hat{c}_c^\dagger - \hat{c}_i \hat{c}_c)$$

where, $\hat{c}_i^\dagger$ and $\hat{c}_i$ are creation and annihilation operators, respectively, defined in the eigen-basis of the corresponding mode.

Estimation of static ZZ parasitic interaction between the qubits

For two qubits, ZZ interaction originates from interactions between higher levels. It creates error in two qubit gates and is a major problem for scalability. It can be quantified as,

$$ZZ = E_{101} - E_{001} - E_{100} - E_{000},$$

where, E_m denotes the eigen-energy of state $|m\rangle$. Using numerical simulations, ZZ interaction strength has been obtained and plotted with coupler frequency and Q_2 frequency in Fig.10.

With respect to Q_2 frequency, the region with detuning $|\omega_1 - \omega_2| <$ anharmonicity $|\alpha|$, is known as straddling region.

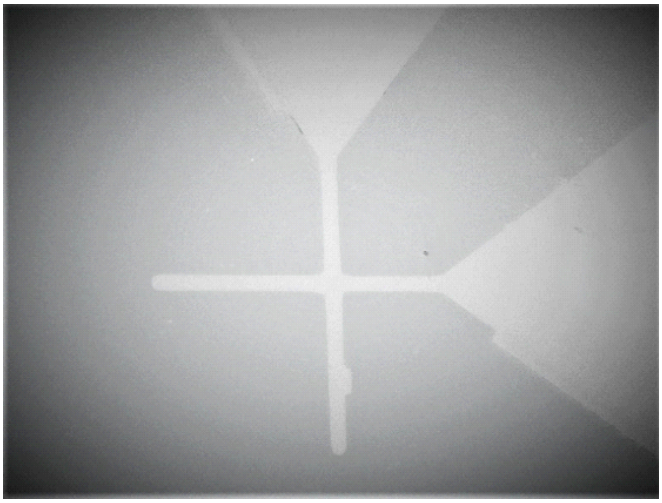

Fig.12: (b) SEM image of fabricated Josephson junction.

Otherwise, it is known as non-straddling region. The light green coloured regions in the straddling regime indicate cancellation of ZZ interaction. This condition is observed when coupler is biased at much higher frequency than qubits, and detuning is less than anharmonicity.

iSwap gate

To implement iswap gate, interaction between the qubits has to be created. If g is coupling strength between the qubits then the swapping time is given by π/2g. At coupler frequency 4.3 GHz, the effective coupling strength between the qubits at 4 GHz is approximately 45 MHz giving a swapping time of nearly 35ns.

In the simulations, the coupler frequency is first set to 5.19 GHz, where both qubits are isolated from each other. Under this idling state, with interaction between qubits nearly zero, Q_1 is excited to create state |100>. Subsequently, frequency of second qubit is changed such that states |100> and |001> become degenerate. The interaction between qubits is increased by changing the coupler frequency to 4.3 GHz. As shown in Fig.11, we need to wait about 34.7 ns for complete exchange from |100> to |001>.

Fabrication of the Quantum Chip

Presently, fabrication trials of the designed device are in progress and the process is being optimized. The Fig.12 (a) and Fig.12 (b) show the Optical and SEM image of the fabricated design and Josephson Junction, respectively.

Conclusions

Results of the simulations, performed to design components on the superconducting chip, have been presented. Effect of the change in the coupler frequency on the coupling between qubits is obtained. Also, the always on static ZZ parasitic interaction has been estimated. Two qubit iSwap gate operation using tunable coupler has been demonstrated. On-going work includes obtaining optimal control drive for the gate implementation, package simulations and fabrication of the chip.

Acknowledgments

The authors would like to thank, Prof. Shiv Govind Singh, IIT Hyderabad, and Prof. Ammanabrolu Rajini kanth, University of Hyderabad for all the technical discussions and facilitating the fabrication trails. Additionally, the authors deeply appreciate the QuMaC team for providing technical guidance and support.

References

[1] M. Hatridge, et al., Physical Review B 83, 134501 (2011).

[2] S. Barzanjeh, et al., Science 363, 6373 (2019).

[3] D. Vion, et al.,Science 296, 886 (2002).

[4] J. M. Chow, et al.,Phys. Rev. A 82, 040305(2010).

[5] J. M. Chow,et al.,Phys. Rev. Lett. 109, 060501 (2012).

[6] Y. Makhlin, et al.,Rev. Mod. Phys. 73, 357 (2001).

[7] M.A. Nielsen and I.L. Chuang, Quantum Computation and Quantum Information (Cambridge University Press, 2000)

[8] A. Blais, et al., Phys. Rev. A, 69,6 (2004).

[9] A. Frank et al., Nature, 574,7779(2019).

[10] M. H. Devoret, et al., Science, 339(2003).

[11] F. Yan, et al., Appl. Phys. Rev. 10, 054062 (2018)

[12] Y. Sung, et al., Phys. Rev. X,11 (2021)

[13] P. Krantz, et al., Appl. Phys. Rev. 6, 021318 (2019).

[14] Z.K. Minev, et al., Qiskit metal: An open-source framework for quantum device design& analysis, Generic, (2021)

[15] J.M. Chow, Quantum Information Processing with Superconducting Qubits, Ph.D Thesis, Yale University, May 2010

[16] S.E. Nigg, et al., Phys. Rev. Lett. 108, 240502 (2012)

[17] D.T. Sank, Fast, Accurate State Measurement in Superconducting Qubits, Ph.D. Thesis, University of California Santa Barbara, September 2014.

[18] J.Johansson, et al., Computer Physics Communications, 184 (2013).